Title
PET radiotracer development for imaging high-affinity state of dopamine D2 and D3 receptors: Binding studies of fluorine-18 labeled aminotetralins in rodents

Journal
Synapse, 71(3)

ISSN
0887-4476

Authors
Mukherjee, Jogeshwar
Majji, Divya
Kaur, Jasmeet
et al.

Publication Date
2017-03-01

DOI
10.1002/syn.21950

Peer reviewed

HHS Public Access

Author manuscript

Synapse. Author manuscript; available in PMC 2018 March 01.

Published in final edited form as:

Synapse. 2017 March ; 71(3): . doi:10.1002/syn.21950.

PET radiotracer development for imaging high-affinity state of dopamine D2 and D3 receptors: Binding studies of fluorine-18 labeled aminotetralins in rodents

Jogeshwar Mukherjee[1], **Divya Majji**[1], **Jasmeet Kaur**[1], **Cristian C. Constantinescu**[1], **Tanjore K. Narayanan**[2], **Bingzhi Shi**[2], **Mohamed T. Nour**[1], and **Min-Liang Pan**[1]

[1]Department of Radiological Sciences, Preclinical Imaging Center, University of California-Irvine, Irvine, California 92697, USA

[2]Department of Nuclear Medicine, Kettering Medical Center, Dayton, Ohio 45429, USA

Abstract

Imaging the high-affinity, functional state (HA) of dopamine D2 and D3 receptors has been pursued in PET imaging studies of various brain functions. We report further evaluation of ^{18}F-5-OH-FPPAT, and the newer ^{18}F-5-OH-FHXPAT and ^{18}F-7-OH-FHXPAT. Syntheses of ^{18}F-5-OH-FHXPAT and ^{18}F-7-OH-FHXPAT were improved by modifications of our previously reported procedures. Brain slices and brain homogenates from male Sprague-Dawley rats were used with the 3 radiotracers (74–111 kBq/cc). Competition with dopamine (1–100 nM) and Gpp(NH)p (10–50 μM) were carried out to demonstrate binding to dopamine D2 and D3 HA-states and binding kinetics of ^{18}F-5-OH-FPPAT measured. Ex vivo brain slice autoradiography was carried out on rats administered with ^{18}F-5-OH-FHXPAT to ascertain HA-state binding. PET/CT imaging in rats and wild type (WT) and D2 knock-out mice were carried out using ^{18}F-7-OH-FHXPAT (2–37 MBq). Striatum was clearly visualized by the three radiotracers in brain slices and dopamine displaced more than 80% of binding, with dissociation rate in homogenates of 2.2×10^{-2} min^{-1} for ^{18}F-5-OH-FPPAT. Treatment with Gpp(NH)p significantly reduced 50–80% striatal binding with faster dissociation rates (5.0×10^{-2} min^{-1}), suggesting HA-state binding of ^{18}F-5-OH-FPPAT and ^{18}F-5-OH-FHXPAT. Striatal binding of ^{18}F-5-OH-FHXPAT in ex vivo brain slices were sensitive to Gpp(NH)p, suggesting HA-state binding in vivo. PET binding ratios of ^{18}F-7-OH-FHXPAT in rat brain were ventral striatum/cerebellum=2.09 and dorsal striatum/cerebellum=1.65; similar binding ratios were found in the D2 WT mice. These results suggest that in vivo PET measures of agonists in the brain at least in part reflect binding to the membrane-bound HA-state of the dopamine receptor.

Keywords

autoradiography; dopamine receptor; fluorinated agonists; high-affinity state; PET

Correspondence: Jogesh Mukherjee, Ph. D., Preclinical Imaging, B138 Medical Sciences, Department of Radiological Sciences, University of California-Irvine, Irvine, CA 92697-5000, USA. j.mukherjee@uci.edu.
Present address Cristian C. Constantinescu, Molecular Neuroimaging, New Haven, CT, USA

CONFLICT OF INTEREST

The authors declare no conflict of interest in the work presented here.

1 | INTRODUCTION

Agonist imaging is able to provide information on functional dopamine receptors. Several agonists have been pursued for in vivo imaging. Aminotetralins, ^{11}C-5-OH-DPAT, ^{11}C-PPHT, ^{11}C-ZYY339, and ^{18}F-5-OH-FPPAT have been reported by us for successful PET imaging of dopamine receptors (Mukherjee et al., 2000, 2004; Shi et al., 1999, 2004). Depending on the position of the phenolic hydroxyl (5- or 7), the aminotetralins can exhibit higher affinity for D2 while maintaining a similar affinity for D3 receptors (Figure 1, **1**). Apomorphine analogs, ^{11}C-NPA in PET studies of nonhuman primates clearly showed binding to the caudate-putamen, similar to that found for ^{11}C-raclopride (Finnema et al., 2009; Hwang et al., 2005). More recently, agonists ^{18}F-MCL-524, apomorphine analogs (Finnema et al., 2014; Sromek et al., 2014) and ^{18}F-aminomethylchroman analogs (Shalgunov et al., 2015a,b) have been reported for imaging dopamine D2 and D3 receptors. ^{11}C-PHNO is a modified aminotetralin derivative and has high-affinity for D2 and D3 receptor subtypes thus suggesting that PHNO binds to D2-high affinity state (HA) and D3 receptors. Along with binding to the caudate-putamen, binding appears to be greater in the globus pallidus indicating a possible D3-preferred binding (Seeman et al., 2006; Tziortzi et al., 2011; Willeit et al., 2006).

Selective agents are needed for both the D2 receptor subtype and D3 receptor subtype. Efforts have been made to identify the D3 receptor binding component of well-known imaging agents, such as ^{18}F-fallypride (e.g., Mukherjee et al., 2015). The role of dopamine D3 receptors in addiction is becoming increasingly important and may thus be a target in the treatment of addictive behaviors (Le Foll et al., 2014; Payer et al., 2014). Efforts are being made to evaluate D3 specific antagonists for treatment of addiction (Mugnaimi et al., 2013). In addition, there is now an increasing body of evidence to suggest the D3 receptor as a potential therapeutic target for antipakinsonian drugs (Joyce and Millan, 2005). Studies have demonstrated an up-regulation of the D2 receptor and down-regulation of the D3 receptor in Parkinson's Disease (Levesque et al., 1992; Vuckovic et al., 2010). Therefore, selective D2 and D3 receptor imaging agents will be more useful in evaluating efficacy of treatment regimens. Development of selective agents have been actively pursued; successful aminotetralin-based, piperazine-based, apomorphine-based compounds have been reported (e.g., Mach et al., 2011; Mukherjee et al., 2000; Shi et al., 2004; Sromek et al., 2014).

Our previous results with ^{18}F-fluorinated aminotetralin, ^{18}F-5-OH-FPPAT showed promising in vivo imaging and selective binding in vitro to the HA- state of the dopamine receptors (Mukherjee et al., 2004; Shi et al., 2004). We report two new analogs of ^{18}F-5-OH-FPPAT, namely ^{18}F-5-OH-FHXPAT **3** which has an additional carbon extending the distance between the nitrogen and fluorine and ^{18}F-7-OH-FHXPAT **4,** which has the phenolic hydroxyl at the 7-position, an analog of 7-OH-DPAT, known to bind selectively to D3 receptors (7-OH-DPAT is 100 fold more selective for D3R, van Vliet et al., 1996). Our goal in this article was to evaluate the binding properties of these three agonists, ^{18}F-5-OH-FPPAT **2**, ^{18}F-5-OH-FHXPAT **3,** and ^{18}F-7-OH-FHXPAT **4** (Figure 1), to assess competition with dopamine, kinetics of association and dissociation, demonstration of binding to HA-

state of the receptor in vitro and ex vivo and preliminary in vivo PET imaging of ^{18}F-7-OH-FHXPAT in rats and mice.

2 | MATERIALS AND METHODS

All chemicals and solvents were of analytical or HPLC grade from Sigma-Aldrich Chemical Co. and Fisher Scientific. Electrospray mass spectra were obtained on a Model 7250 mass spectrometer (Micromass LCT). Proton NMR spectra were recorded on a Bruker Cryo 500 MHz spectrometer. Analytical thin layer chromatography (TLC) was carried out on silica coated plates (Baker-Flex, Phillipsburg, NJ). Chromatographic separations were carried out on preparative TLC (silica gel GF 20 × 20 cm 2000 μm thick; Alltech Assoc., Deerfield, IL) or silica gel flash columns or semi-preparative reverse-phase columns using the Gilson high performance liquid chromatography (HPLC) systems. High specific activity ^{18}F-fluoride was produced either in the MC-17 cyclotron or RDS 112 cyclotron using oxygen-18 enriched water (^{18}O to ^{18}F using p, n reaction) and was used in subsequent reactions which were carried out in automated radiosynthesis units [chemistry processing control unit (CPCU)]. Fluorine-18 radioactivity was counted in a Capintec dose calibrator while low level counting was carried out in a well-counter (Cobra quantum, Packard Instruments, Boston, MA). Rat brain slices were cut in a Leica 1850 cryotome. Fluorine-18 autoradiographic studies were carried out by exposing tissue samples on storage phosphor screens. The apposed phosphor screens were read and analyzed by OptiQuant acquisition and analysis program of the Cyclone Storage Phosphor System (Packard Instruments, Boston, MA). A preclinical Inveon dedicated PET/CT scanner (Siemens Medical Solutions, Knoxville, TN) with a transaxial full width half maximum (FWHM) of 1.46 mm, and axial FWHM of 1.15 mm (Constantinescu and Mukherjee, 2009) was used for the PET studies. PET images were analyzed using ASIPro and Inveon Research Workplace (from Siemens Medical Solutions, Knoxville, TN) and PMOD software (PMOD Technologies, Switzerland). All animal studies were approved by the University of California Irvine Institutional Animal Care and Use Committee (IACUC) or Wright State University IACUC.

2.1 | Radiosynthesis

2.1.1 | 2-(N-propyl-N-5′-^{18}F-fluoropentyl)amino-5-hydroxytetralin (2) (^{18}F-5-OH-FPPAT)—The synthesis of ^{18}F-5-OH-FPPAT was carried out using previously reported methods (Shi et al., 2004). ^{18}F-5-OH-FPPAT was typically obtained in specific activity >74 MBq/nmol in ~185–370 MBq batches for imaging studies. The final sterile 0.9% saline solution of ^{18}F-5-OH-FPPAT, pH in the range of 6–7, was dispensed for in vitro and in vivo studies.

2.1.2 | 2-(N-propyl-N-6′-^{18}F-fluorohexyl)amino-5-hydroxytetralin (3) (^{18}F-5-OH-FHXPAT)—High specific activity fluorine-18 was solubilized using Kryptofix and potassium carbonate. It was evaporated to dryness using anhydrous acetonitrile. The brominated precursor **5** (Figure 2a; prepared using modifications of procedures described in Shi et al., 2004) was added (1 mg in 1 mL acetonitrile) and reacted at 96°C for 20 min. Following the reaction, any unreacted ^{18}F-fluoride was removed by adding methanol to the mixture and passing the methanolic contents (containing 2-(*N*-propyl-*N*–5′-^{18}F-

fluorohexanoyl)amino-5-tetrahydropyranyltetralin) through a neutral alumina seppak out of the CPCU. The methanol was removed under vacuum and lithium aluminum hydride (LAH; 0.2 mL of 1.0 M in THF) was added to reduce the amide product. After 5 min at room temperature, hydrochloric acid (0.5 mL of 1 N HCl) was added to quench the unreacted LAH and to deprotect the tetrahydropyranyl ether. The mixture was left to react at 80°C for 15 min and then cooled to ambient temperature, quenched with saturated sodium bicarbonate solution, and extracted with methylene chloride. The organic extract was evaporated and the residue was purified by HPLC. The retention time of ^{18}F-5-OH-FHXPAT **3** was found to be 24.0 min using the solvent of 60% acetonitrile, 0.25% triethylamine in water at a flow rate of 2.0 mL/minute (Figure 2a). The radiosynthesis was accomplished in 2 hr with a decay corrected overall radiochemical yield of ~5–10%. The specific activity of the radiotracer was estimated to be >74 MBq/ nmol.

Partition of ^{18}F-5-OH-FHXPAT between octanol and 0.066 M phosphate buffered saline, pH 7.4 was carried out in order to estimate lipophilicity as described previously (Shi et al., 1999). The log P of ^{18}F-5-OH-FHXPAT was found to be 1.80.

2.1.3 | 2-(N-propyl-N-6′-^{18}F-fluorohexyl)amino-7-hydroxytetralin (4) (^{18}F-7-OH-FHXPAT)—

As described above, high specific activity fluorine-18 was reacted with the precursor 2-(*N*-propyl-*N*–6′-bromohexyl)amino-7-tetrahydropyranyltetralin **6**, (Figure 2b; prepared using modifications of procedures described in Shi et al., 2004). Fluorine-18 was solubilized using Kryptofix and potassium carbonate and evaporated to dryness using anhydrous acetonitrile. Subsequently, the bromo precursor **6** (1 mg in 1 mL of anhydrous acetonitrile) was added and the reaction went for 20 min at 96°C. Following the reaction, methanol was added to the mixture and the methanolic contents were passed through a neutral alumina seppak (prewashed with methanol) out of the CPCU. This removed any unreacted ^{18}F-fluoride and the methanolic solution now contained 2-(*N*-propyl-*N*–6′-^{18}F-fluorohexyl)amino-7-tetrahydropyranyltetralin. The methanol was removed in vacuo, and hydrochloric acid (0.5 mL of 1N HCl) was added to deprotect the tetrahydropyran. The reaction proceeded at 80°C for 15 min. The contents were then cooled to ambient temperature, quenched with 0.8 mL of 1.0 M sodium bicarbonate solution, extracted with methylene chloride. The organic extract was evaporated and the residue was taken up for HPLC purification. The retention time of ^{18}F-7-OH-FHXPAT was found to be 20 min using the solvent of 60% acetonitrile, 0.25% triethylamine in water at a flow rate of 2.5 mL/minute (Figure 2b). The radiosynthesis was accomplished in 2 hr from end of bombardment with a decay corrected overall radiochemical yield of 10–15%. The specific activity of the radiotracer was estimated to be >74 MBq/nmol.

2.2 | In vitro autoradiographic studies

Rat brain tissue horizontal sections slices (10 μm thick) were removed from storage and allowed to come to room temperature (22–25°C) over a period of 15–30 min. The tissue sections were placed in 50 mM Tris HCl buffer (pH 7.4, 25°C) containing 120 mM NaCl and 5 mM KCl and were preincubated for 15 min. Following incubation with the respective radiotracer, tissue sections were briefly washed twice for 1 min period each with cold 50 mM Tris HCl buffer, pH 7.4, followed by a quick rinse in cold deionised water. After

washing, tissue sections were dried under a cool stream of air. Tissue sections were then apposed to storage phosphor screens (Packard Instruments) and left for overnight exposure. Autoradiograms were read and analyzed using the Cyclone Storage Phosphor System (Packard Instruments).

2.2.1 | ^{18}F-5-OH-FPPAT—The preincubated slices were incubated in fresh buffer with ^{18}F-5-OH-FPPAT, 111 kBq/cc at concentrations of ~1 nM for 60 min at 25°C for total binding and with different concentrations of dopamine (final concentrations of 1, 10, and 100 nM).

2.2.2 | ^{18}F-5-OH-FHXPAT—The preincubated slices were incubated in fresh buffer with ^{18}F-5-OH-FHXPAT 74 kBq/cc at concentrations of ~1 nM for 60 min at 25°C for total binding. In the case of experiments with 5′-guanylylimidophosphate (Gpp(NH)p), which is known to convert the HA-sites to LA-sites (Grigoriadis and Seeman, 1985), brain slices were preincubated for 15 min at 25°C with the above mentioned buffer containing 42 μM of Gpp(NH)p and subsequently ^{18}F-5-OH-FHXPAT 74 kBq/cc was added. Nonspecific binding was defined as the binding remaining in the presence of 10 μM (*S*)-sulpiride. In a separate set of experiments, brain slices were incubated with different concentrations of dopamine (final concentrations of 1, 10, and 100 nM).

In vitro effect of isoflurane on the binding of ^{18}F-5-OH-FHXPAT was evaluated by incubating brain slices in buffer containing 0.1, 1, and 2% isoflurane (v/v). Horizontal brain slices (20 μm thick) were first pre-incubated for 15 min in the above isoflurane containing buffers, after which incubation was carried out along with ^{18}F-5-OH-FHXPAT (15 kBq/cc) for 1 hr at 37°C. After 60 min, the processing of the slides was carried as described above.

2.2.3 | ^{18}F-7-OH-FHXPAT—In order to measure total in vitro binding, the preincubated sections were incubated in fresh buffer with ^{18}F-7-OH-FHXPAT 74 kBq/cc for 60 min at room temperature. Binding was also carried out in the presence of 10 μM SKF 10047 and 100 nM dopamine, to assess binding to sigma receptors and competition of ^{18}F-7-OH-FHXPAT with dopamine. Non-specific binding was measured in the presence of 10 μM haloperidol.

2.3 | In vitro kinetics of ^{18}F-5-OH-FPPAT

2.3.1 | Association kinetics of ^{18}F-5-OH-FPPAT—Male Sprague-Dawley rats (200–250 g) were sacrificed and brain homogenate was prepared as previously reported (Shi et al., 1999). For association kinetics, the incubation mixture consisted of 0.10 mL of ^{18}F-5-OH-FPPAT (37 kBq/cc; specific activity >74 MBq/nmol), 0.80 mL of buffer, and 0.10 mL of tissue (stock of 10 mg/mL) to provide a total incubation volume of 1.0 mL. Two additional sets of association experiments were carried out in the presence of Gpp(NH)p (5 and 50 μM final concentrations). The mixtures were incubated at 25°C. Binding was initiated by adding tissue homogenate to the incubation mixture at various times (range between 1 and 120 min) followed by filtration using Brandel filtration apparatus of the incubation mixtures followed by 3 × 5 mL washes with cold buffer. Nonspecific binding was measured using 100 μM of sulpiride. The association rate constant was computed to be $M^{-1}min^{-1}$ from $K_1 = K_{obs} - K_{-1}/$

[*M*], where K_1 is the association rate constant, K_{obs} is the observed rate constant, K_{-1} is the dissociation rate constant and [*M*] is the concentration of the radio ligand.

2.3.2 | Dissociation kinetics of ^{18}F-5-OH-FPPAT—Dissociation kinetics was carried out under similar concentrations of tissue and ^{18}F-5-OH-FPPAT (37 kBq/cc). The mixtures were incubated for 1 hr at 25°C. The dissociation of ^{18}F-5-OH-FPPAT was initiated by adding an excess of dopamine (10 μM final concentration), 5-OH-FPPAT (10 μM final concentration), or Gpp(NH)p (50 μM final concentration) in time range of 1–60 min. The incubation was terminated by filtration through Whatman GF/B filters presoaked in 0.3% polyethylenimine, with a Brandel model M-24R cell harvester. The filters were rinsed for 10 s with ice-cold Tris-HCl buffer, and the filters were counted for fluorine-18 using an Auto-Gamma 5000 (Packard Instruments).

2.4 | Ex vivo autoradiographic studies of ^{18}F-5-OH-FHXPAT

Male Sprague-Dawley rats (250–300 g; *n*=3) were fasted 18 hr prior to time of study. On the day of the study, rats were anesthetized using 3.0% isoflurane. ^{18}F-5-OH-FHXPAT (7–15 MBq) was injected intravenously in the tail as 0.3 mL bolus. After injection, the animals were placed back in their cage allowed to recover and be awake. Twenty-five minutes post injection of ^{18}F-5-OH-FHXPAT, the animals were anesthetized again and killed by decapitation. The brain was rapidly removed and prepared for sectioning. Ex vivo coronal rat brain slices were prepared at 20 μm thick using a Leica 1850 cryotome. Select sections were treated with either buffer, buffer containing 10 μM dopamine or buffer containing 50 μM Gpp(NH)p for 12 min. After drying the sections, fluorine-18 autoradiograms were obtained by exposing tissue samples overnight on storage phosphor screens (Perkin Elmer Multisensitive, Medium MS). The apposed phosphor screens were read and analyzed by Optiquant acquisition and analysis program of the Cyclone Storage Phosphor System (Packard Instruments, Boston, MA). Region-of-interest of same size were drawn on brain slices and analyzed using Optiquant software and binding of ^{18}F-5-OH-FHXPAT measured in Digital Light Units/mm^2 (DLU/mm^2). Ratios of DLU/mm^2 in the striatum to cortex were calculated.

2.5 | Rat PET studies of ^{18}F-7-OH-FHXPAT

Male Sprague-Dawley rats (250–300 g; *n*=3) were fasted 24 hr prior to time of scan. On the day of the study, rats were anesthetized using 4.0% isoflurane. The rats were then positioned on the scanner bed by placing them on a warm-water circulating heating pad and anesthesia applied using a nose-cone. ^{18}F-7-OH-FHXPAT (18–37 MBq) was injected intravenously in the tail as 0.3 mL bolus. Isoflurane was reduced and maintained at 2.5% following injection. PET scans were first done with an Inveon dedicated PET scanner (Constantinescu and Mukherjee, 2009; Siemens Medical Solutions, Knoxville, TN) followed by CT scans with an Inveon Multimodality CT scanner (large area detector, 10 × 10 cm^2 field-of-view, Siemens Medical Solutions, Knoxville, TN). The two scanners were mechanically docked to each other, which allowed sequential PET and CT scanning. Scans were carried out for 60 min and acquired by the Inveon PET in full list mode. The listmode data were rebinned into 3D sinograms of span 3 and ring difference 79. Random events were subtracted prior to reconstruction. The data was histogrammed into 19 frames and reconstructed using Fourier

rebinning and 2D OSEM method with an image matrix of 128 × 128 × 159, resulting in a pixel size of 0.77 mm and a slice thickness of 0.796 mm. Calibration in Bq/cc units was applied using a Ge-68 phantom, which was scanned and reconstructed under the same parameters as the subjects. The CT images were acquired at a binning factor of 4 and were reconstructed using cone-beam reconstruction with a Shepp filter with cutoff at Nyquist frequency resulting in an image matrix of 480 × 480 × 632 and a voxel size of 0.206 mm. All PET data were corrected for random events, scatter and photon attenuation, and for radioactive decay using software provided by scanner manufacturer. PMOD software was used to process images, extract, and analyze time-activity curves from regions of interest drawn on the dorsal striatum (DStr), ventral striatum (VStr), and cerebellum, which was used as reference for nonspecific binding.

2.6 | Mice PET studies of ^{18}F-7-OH-FHXPAT

2.6.1 | PET scanning—All mice for this study were bred and genotyped prior to their use in imaging. D2R knock-out (KO) mice were generated at UCI in the Department of Microbiology and Molecular Genetics following an established procedure (Baik et al., 1995). Mice were housed in individual cages, kept in a climate controlled room (24.4°C), with a 12:12-hr light cycle, and had free access to food and water during housing. Subjects were fasted in the imaging room, in a dark quiet place, for 24 hr prior to the scan. Two wild-type (WT) C57BL/6 mice and two D2 KO mice (male, 30–35 g) from the same generation were acquired and used for the in vivo PET scans.

In preparation for the scans, the animals were anesthetized with isoflurane (4% induction) and then maintained under anesthesia throughout the experiments while in the imaging chamber (2.5% maintenance). Animals were injected with the tracer via tail vein outside the scanner and then quickly positioned inside an imaging chamber (M2M technologies) attached to the scanner bed. PET scans were done first with an Inveon dedicated PET scanner (Siemens Medical Solutions, Knoxville, TN) followed by CT scans as described above.

Mice underwent static ^{18}F-7-OH-FHXPAT (intravenous ~2 MBq) scans for 30 min following a 30 min tracer uptake, under anesthesia. The 30 min uptake period was chosen based on the examination of striatum to cerebellum curves from a rat study, which showed that ^{18}F-7-OH-FHXPAT reached steady-state after 30 min. Images were reconstructed with Fourier rebinning of 3D data followed by OSEM 2D (16 subsets, 4 iterations, 2 EM iterations). All PET data were corrected for random events, scatter and photon attenuation.

2.6.2 | Data analysis—Processing of reconstructed images and data analysis were performed with PMOD software package (PMOD Technologies). All PET images were co-registered to an MRI brain template (Ma et al., 2008). The CT images were resliced and manually coregistered via rigid transformations (translations and rotations) to match the template using PMOD Fusion toolbox. A head-and-hat approach was taken for coregistration with using the skull and brain shape features visible in CT and MR template, respectively. The resulting rigid transformation matrix for each subject was subsequently applied to all the PET images to achieve coregistration to the MR template. 3D volumes of

interest (VOIs) representing DStr, VStr, and cerebellum were drawn on the template. The VOIs on DStr and VStr consisted of spheres of 1 mm diameter placed symmetrically left and right with respect to midline (2×0.52 mm^3), scaled down versions of VOIs used previously for the rat brain for these structures (Constantinescu et al., 2011). The cerebellum VOI consisted of one sphere of 2 mm diameter (3.85 mm^3) placed centrally on the structure. The left and right values in VOIs for each structure were combined into a single VOI. All VOIs were transferred to PET images and the mean VOI activity were extracted for each brain region. The tissue ratios between regions with specific binding and cerebellum were computed.

3 | RESULTS

3.1 | Radiosynthesis

Fluorine-18 displacement of the two different THP-protected bromo-precursors proceeded in moderate radiochemical yields. For ^{18}F-5-OH-FPPAT and ^{18}F-5-OH-FHXPAT, our previously reported 3-step procedure was followed (Shi et al., 2004). This included radiolabeling the precursor with fluorine-18, reducing the amide to an amine and removal of the THP group under mild conditions. Radiochemical yields of ^{18}F-5-OH-FHXPAT were in the 10% range decay corrected. The reduction step using LAH was found to be cumbersome and difficult to automate. The modified radiosynthesis of ^{18}F-7-OH-FHXPAT, which required two steps was developed. The first step is the ^{18}F-fluoride nucleophilic displacement of the bromo substituent and the second step involved removal of the THP group. The reduction step was eliminated and the overall radiosynthesis was found to be much cleaner and easier to automate.

3.2 | In vitro studies

3.2.1 | ^{18}F-5-OH-FPPAT—Selective binding of ^{18}F-5-OH-FPPAT was observed in the striata in vitro in rat brain slices while little binding was observed in the cerebellum (Figure 3a). Cortical areas did show some binding as seen in Figure 3a. Nonspecific binding was measured using sulpiride (10 μM), which was able to block in excess of 90% of the selective binding of ^{18}F-5-OH-FPPAT in the striata. The binding of ^{18}F-5-OH-FPPAT was also selectively inhibited in vitro by various concentrations of dopamine (Figure 3). The striata to frontal cortex ratio in the control slice was found to be 14.2. This ratio went down to 9.37 for 1 nM dopamine, 5.27 for 10 nM dopamine, and 2.8 for 100 nM dopamine. Dopamine was thus able to progressively compete with the binding of ^{18}F-5-OH-FPPAT with about 80% of it displaced in the presence of 100 nM (Figure 3b).

In vitro association and dissociation experiments in rat brain tissue with ^{18}F-5-OH-FPPAT were analyzed using kinetic EBDA analysis (Munson and Rodbard, 1980). All in vitro homogenate binding experiments were carried out at 25°C. The observed association rate constant measured from the data shown in Figure 3c was found to be 0.13 min^{-1}. In the presence of 5 and 50 μM Gpp(NH)p, an ~50% reduction in specific binding of ^{18}F-5-OH-FPPAT in rat brain homogenates was observed. The association rate, however, was similar to that observed in the control set of experiments (Figure 3c).

Dissociation of specifically bound ^{18}F-5-OH-FPPAT was initiated at equilibrium (after 60 minutes of incubation of ^{18}F-5-OH-FPPAT with tissue homogenate) by 10 μM dopamine and by 10 μM 5-OH-FPPAT (Figure 3d). The dissociation of ^{18}F-5-OH-FPPAT was relatively rapid and at 60 min >80% of ^{18}F-5-OH-FPPAT was displaced with a dissociation rate of 0.02 min^{-1}. Dissociation of ^{18}F-5-OH-FPPAT was also induced by adding 50 μM Gpp(NH)p. Rapid dissociation of ^{18}F-5-OH-FPPAT was observed within the first 8 min with rates of 0.05 min^{-1} during which only ~40–45% of ^{18}F-5-OH-FPPAT was displaced (Figure 3d). Subsequently, no further dissociation of ^{18}F-5-OH-FPPAT occurred.

3.2.2 | ^{18}F-5-OH-FHXPAT—Similar to the binding of ^{18}F-5-OH-FPPAT, localization of ^{18}F-5-OH-FHXPAT occurred in the striata in vitro in rat brain slices as seen in Figure 4a. Other regions of the brain did not show any significant amount of binding. Sulpiride (10 μM) was able to block >95% of the selective binding of ^{18}F-5-OH-FHXPAT in the striata (Figure 4c). In the presence of Gpp(NH)p (42 μM), the receptors were converted to their low affinity state, thus reducing the binding of ^{18}F-5-OH-FHXPAT substantially (>80%; Figure 4b).

The binding of ^{18}F-5-OH-FHXPAT was also selectively inhibited in vitro by various concentrations of dopamine (Figure 4d). Binding in the striata of control slice was reduced by 21% in the presence of 1 nM dopamine. With increasing dopamine concentration to 10 nM, there was a 74% reduction in striatum binding of ^{18}F-5-OH-FHXPAT and plateaued at 100 nM dopamine. Dopamine was thus able to progressively compete with the binding of ^{18}F-5-OH-FHXPAT with >75% displaced by 100 nM dopamine (Figure 4e).

3.2.3 | ^{18}F-7-OH-FHXPAT—Binding of ^{18}F-7-OH-FHXPAT occurred in the striata and other brain regions in vitro in rat brain slices as seen in Figure 5a. In the presence of 10 μM SKF10047, a sigma-1 receptor ligand, 55% of the binding of ^{18}F-7-OH-FHXPAT was reduced over the various brain regions (Figure 5b). Significant ^{18}F-7-OH-FHXPAT remained bound in the striata. However, binding of ^{18}F-7-OH-FHXPAT to the striata was displaced in the presence of SKF10047 and 100 nM dopamine (Figure 5c). Haloperidol (10 μM) displaced >95% binding of ^{18}F-7-OH-FHXPAT from all regions of the brain (Figure 5d).

3.3 | Ex vivo distribution studies in rats

Ex vivo autoradiography of coronal sections (20 μm thick) through the striatum showed localization of the radiotracer in the dorsal and ventral striata (Figure 6a). Lower amounts of binding were observed in the cortex. The ex vivo binding was similar to the in vitro striatal binding of ^{18}F-5-OH-FHXPAT in coronal slices (Figure 6b). The striata to cortex ratios were ~1.5–1.6.

To assess displaceability of ^{18}F-5-OH-FHXPAT in the ex vivo sections, treatment of the sections with buffer solution only, buffer containing 10 μM dopamine, and buffer containing 50 μM Gpp(NH)p had varying effect. In one set, buffer containing 10 μM dopamine, and buffer containing 50 μM Gpp(NH)p were applied only to one-half of the brain and in both the cases there was a reduction in the binding. To ascertain that this was not simply a displacement effect due to the dilution effect of added buffer, the buffers were added to the entire slice, along with the control buffer with no drug. Dopamine had the greatest

displacing effect (striata to cortex ratios before drug was 1.5–1.6, which decreased by >80%), whereas Gpp(NH)p reduced it by >45%, compared with the control buffer.

3.4 | In vivo rat PET studies

Figure 7 shows brain uptake of ^{18}F-7-OH-FHXPAT in control rats. Brain uptake in the rats was rapid in both the cerebrum and cerebellum in both the rats shown (Figure 7j,k). Preferential localization of ^{18}F-7-OH-FHXPAT was seen in the striatum compared with the cerebellum and in both the animals, the clearance of ^{18}F-7-OH-FHXPAT from these brain regions was similar. Coregistration with the rat MR template (Figure 7a–c) was carried out to assist in identifying regional brain localization of ^{18}F-7-OH-FHXPAT. Binding of ^{18}F-7-OH-FHXPAT was evident in both the dorsal and ventral striata (Figure 7d–f) and this was confirmed by the coregistered images in Figure 7g–i. The ventral striata exhibited marginally greater binding of ^{18}F-7-OH-FHXPAT, which was also evident in the time activity curves. Clearance from cerebellar lobes was faster, although greater activity was seen in the midline regions and brain stem. Average ratios of VStr to cerebellum at 55 min was 2.09 and that of DStr, to cerebellum was 1.65 at 55 min (Figure 7j,k).

3.5 | In vivo mice PET studies

Brain uptake images of ^{18}F-7-OH-FHXPAT acquired at 30 min post tracer injection are shown in Figure 8. The MR coregistered images shown in Figure 8b,c indicate the distribution of ^{18}F-7-OH-FHXPAT to be similar in both WT and KO mouse brain. The levels of ^{18}F-7-OH-FHXPAT in the cerebellum were similar as seen in Figure 8e. Binding of ^{18}F-7-OH-FHXPAT in both WT and KO mice was moderate, with DStr to cerebellum ratios of 1.57 for WT and 1.41 for the KO. Ratios of VStr to cerebellum ratios were a little higher, with 2.06 for WT and 1.64 for KO (Figure 8d). Thus, the VStr had a higher ratio for both mouse types.

3.6 | In vitro anesthesia effects

Measurement of effects of isoflurane on the binding of ^{18}F-5-OH-FHXPAT in vitro revealed a significant reduction in the binding in the striata (Figure 9a). The striata to cerebellum ratio in the control slice was found to be 11.1 (Figure 9b). This ratio went down to 7.82 in the presence of 0.1% isoflurane (30% reduction), 3.56 for 1% isoflurane (a reduction of 68%), and 3.03 for 2% isoflurane (a reduction of 73%). Thus, isoflurane progressively decreased the binding of ^{18}F-5-OH-FHXPAT in the striata in vitro.

4 | DISCUSSION

In continuation with our successful PET imaging of dopamine D2-like receptor agonists radiolabeled with carbon-11 (Mukherjee et al., 2000, 2004; Shi et al., 1999), we embarked on the development of fluorine-18 agonist analogs as dopamine D2-like receptor PET imaging agents. Our initial efforts developed ^{18}F-5-OH-FPPAT (Shi et al., 2004), which showed promising in vitro properties for binding to the high-affinity state of the receptors in the striatum in vitro and the ability to localize to the dopamine receptors in vivo. Because of this success, we proceeded to make two additional analogs, first by extending the fluoroalkyl chain to six carbons so that ^{18}F-5-OH-FHXPAT was made (which increased its lipophilicity

from log *P* of 1.60 for ^{18}F-5-OH-FPPAT to log *P* of 1.80 for ^{18}F-5-OH-FHXPAT), which may allow greater brain uptake and second, we moved the position of the phenolic hydroxyl from the 5-position to the 7-position so that ^{18}F-7-OH-FHXPAT was made, which becomes an analog of 7-OH-DPAT, a D3 receptor preferring agent. The 5-hydroxy derivatives were prepared with our reported older method involving 3-steps (Shi et al., 2004), whereas the 7-hydroxy derivative was prepared by a newer 2-step method reported here, which provides somewhat higher radiochemical yields and is less cumbersome. The availability of the three radiotracers allowed us to carry out a series of biological experiments to study their binding to the dopamine receptors in vitro, ex vivo and in vivo.

All the three radiotracers, ^{18}F-5-OH-FPPAT, ^{18}F-5-OH-FHXPAT, and ^{18}F-7-OH-FHXPAT, localized in the striatum of rat brain slices in vitro as observed in the autoradiographs (Figures 3–5). Ratios of binding between striatum and cerebellum were highest for ^{18}F-5-OH-FPPAT, thus suggesting that the two modifications of chain length and position of the hydroxyl group do not necessarily improve in vitro binding. In the case of ^{18}F-7-OH-FHXPAT nonspecific binding was reduced in the presence of a sigma-1 receptor inhibitor and may be consistent with previous reports of 7-OH-PIPAT exhibiting such behavior (Kung et al., 1994). The use of the pure *R*-isomer is likely to alleviate the problem of this sigma-1 receptor binding, since the (*S*)-isomer, such as in ^{125}I-(*S*)–7-OH-PIPAT has been shown to bind to sigma receptors (Garner et al., 1994).

Dopamine displaced all the three radiotracers from the striata in brain slices. At 10 nM dopamine concentrations, displacement approached 70%, and 100 nM dopamine caused ~80% displacement of the radiotracers. Dissociation of ^{18}F-5-OH-FPPAT in rat brain homogenates with dopamine was rapid with dissociation rate constants of 2.2×10^{-2} min^{-1} with most of the bound ^{18}F-5-OH-FPPAT being displaced. This rate of dopamine-induced dissociation was >10-fold faster than observed with antagonist ^{18}F-fallypride dissociation induced by dopamine (100 μM) in rat brain homogenates (^{18}F-fallypride dissociation rate=8.6×10^{-3} min^{-1}; Mukherjee et al., 1997). Dissociation induced by the unlabeled 5-OH-FPPAT of ^{18}F-5-OH-FPPAT in rat brain homogenates also exhibited similar dissociation rate constants as dopamine (2.2×10^{-2} min^{-1}; Figure 3d). This higher degree of displacement of ^{18}F-5-OH-FPPAT by dopamine compared with ^{18}F-fallypride displacement has the potential of being a more sensitive PET imaging tool for measuring in vivo changes in dopamine levels (e.g., Shotbolt et al., 2012).

High-affinity state binding was assessed by using Gpp(NH)p as reported by us before (Shi et al., 1999, 2004). It was also shown that Gpp(NH)p decreased or abolished the binding of ^{3}H-PHNO to the D2 receptors in rat brain slices in vitro (Nobrega and Seeman, 1994). In vitro autoradiographic binding studies of ^{18}F-5-OH-FPPAT and ^{18}F-5-OH-FHXPAT to the HA-state of D2 receptor was confirmed by preincubating the rat brain slices with Gpp(NH)p. In the presence of Gpp (NH)p >80% reduction of binding of the two radiotracers was observed. This is indicative of little or no binding to the low-affinity (LA) state of the D2 receptor. Thus, these experiments confirmed the binding of ^{18}F-5-OH-FPPAT and ^{18}F-5-OH-FHXPAT to the HA-state of the D2 receptor in vitro. The residual binding in the presence of Gpp(NH)p may be due to incomplete conversion of the affinity states, some binding to the low affinity states or internalized radiotracer. It may also reflect some binding to dopamine

D3 receptors which have been shown to be less sensitive to Gpp(NH)p (e.g., Vanhauwe et al., 2000).

Association kinetics of ^{18}F-5-OH-FPPAT in rat brain homogenate tissue and in the presence of two different concentrations of Gpp(NH) p showed significant binding still remained in the presence of Gpp(NH) p. This would suggest that part of the binding of ^{18}F-5-OH-FPPAT is insensitive to Gpp(NH)p and may be due to receptor-ligand complex internalization. The same phenomenon was observed in the case of brain slices although to a lesser degree. It must be noted that in the case of homogenates no preincubation with Gpp(NH)p was done, while brain slices were preincubated for at least 15 min with Gpp(NH)p. Thus, our experiments in the homogenates may point to a partial conversion of the HA-state D2 receptors and a fraction of the D2 HA-state receptors may be present on the membrane surface while a subset of the HA-receptors may be internalized (Figure 10).

In vitro studies have confirmed the presence of HA-state D2 receptor binding of ^{18}F-5-OH-FPPAT and ^{18}F-5-OH-FHXPAT by uncoupling the G-protein complex as described above. The presence of the HA-state in vivo has been difficult to establish (Skinbjerg et al., 2012). Due to blood brain barrier impermeability of Gpp(NH)p, in vivo experiments are difficult to carry out to confirm presence of HA-state. The ex vivo method of using Gpp(NH)p to demonstrate the component of ligand attached to the high-affinity state of the dopamine D2 receptor was earlier used in rat brain homogenates by Seeman (2011). Ex vivo experiments were thus carried out, demonstrating the sensitivity of ^{18}F-5-OH-FHXPAT binding in the striatum to Gpp(NH)p. Like the in vitro experiments, dopamine was able to displace more of ^{18}F-5-OH-FHXPAT compared to Gpp(NH)p. These experiments, although not a substitute for in vivo experiments, suggest the presence of HA-state of D2 receptors in vivo.

We have previously reported successful PET studies with the various 5-hydroxy aminotetralin derivatives (Figure 1) including ^{18}F-5-OH-FPPAT in monkeys. Striatal binding was clearly evident with ratios of ~2 between striatum and cerebellum (Mukherjee et al., 2004). Thus, based on our in vitro and ex vivo observations, it may be surmised that the binding seen in the PET studies is likely to the HA-states of the D2 receptors, perhaps some binding to the D3 receptors and internalized receptors. Because the 7-hydroxy derivatives such as 7-OH-DPAT are more D3-subtype preferring (Mukherjee et al., 2015; van Vliet et al., 1996), PET studies in the rat with ^{18}F-7-OH-FHXPAT demonstrated greater localization of the radiotracer in the VStr, a region known to contain relatively more D3 receptors than D2 receptors. At high specific activities it may be assumed that ^{18}F-7-OH-FHXPAT binding may be predominantly be to D3 subtype, although binding to D2 subtype cannot be ruled out (Gonzalez and Sibley, 1995; Mukherjee et al., 2015). Interestingly, ratio of ventral striata to cerebellum was ~2, similar to that observed with the 5-hydroxy derivatives. The ability of ^{18}F-F-OH-FHXPAT to potentially delineate the D3 receptor in the VStr is very significant.

To verify the binding of ^{18}F-7-OH-FHXPAT to the D3 receptor subtype, we used WT and D2 deficient homozygous (D2 KO) for PET studies. By comparing the KO and WT binding at baseline, similar tissue ratios of ^{18}F-7-OH-FHXPAT in both WT and D2 KO mice were found indicating that ^{18}F-7-OH-FHXPAT binds mostly to D3 receptors. Slightly higher

striatal binding ratios in WT than in KO may possibly be due to a small D2 binding component present in the WT mouse. The largest ratio (~2) was recorded in VStr that has a larger D3 presence. Although the initial evaluation is promising, further blocking studies of ^{18}F-7-OH-FHXPAT with 7-OH-DPAT or other D3 specific drugs need to be performed to completely asses this tracer's specificity to the D3 receptor. These findings are supported by a previous study using autoradiography in mice that showed high ^{11}C-(+)-PHNO binding in these two regions (Rabiner et al., 2009). Using the same animal model, we computed the fraction of ^{18}F-fallypride bound to D3 receptors may be up to 20% (Mukherjee et al., 2015).

There are two major limiting factors that impacted the quantification of mouse images and which need to be taken in account: spillover effects and partial volume effects. The first factor consists of a slowly increasing spillover signal from outside the brain (skull and glands) due to free tracer and/or defluorination, into adjacent brain structures of interest. The maximal scalp/bone uptake was 80–111% of that found in the striatum and 110–130% of that found in the cerebellum. DStr was minimally contaminated by the skull and glands activity due to its deep location inside the brain and away from the skull. We did not employ any methodology aimed to correct for the spillover effects. The cerebellar reference region was placed centrally instead of on the cerebellar lobes. Additionally, based on our in vitro experiments on the binding of agonists in the presence of isoflurane (Figure 9) as well reported findings on the effects of anesthesia on G-protein couple receptors (Seeman and Kapur, 2003), it is anticipated that ^{18}F-hydroxyaminotetralins may provide higher binding in human studies since no anesthesia is involved in the PET studies. However, it must be noted that in vivo experiments with anesthesia actually resulted in an increase in binding of agonists and antagonists (McCormick et al., 2011). Thus, anesthesia effects may be different in vitro versus in vivo and anesthesia effects on endogenous dopamine may influence radiotracer binding in vivo.

Although our findings reported here with the ^{18}F-agonists may be summarized as shown in Figure 10, there are limitations in the study. First, Figure 10 suggests binding of agonists to HA-state in vivo, but we have only demonstrated this in vitro and ex vivo. However, it may be surmised that ex vivo measures do relate to in vivo measures to a good extent. Second, we infer based on differences in the degree of displacement of ^{18}F-agonists by Gpp(NH)p and dopamine, that there is internalization of the receptor. However, since internalization requires several cellular events to occur, it remains to be demonstrated that this may actually occur in the experimental conditions reported here. It remains unclear how dopamine may have access to the internalized ^{18}F-agonist-receptor complex, unless there is rapidly recycling of this complex to the membrane surface or if the exchange is occurring in the internalized complex. Third, our results have not clearly distinguished the D2 and D3 receptor subtypes, although the preliminary findings with the knock out mice suggest a useful tool to identify such receptor subtype selectivity. It may be that the Gpp(NH)p non-displaceable component is actually D3 receptor bound, rather than internalized receptor. Fourth, the selectivity of binding of the three radiotracers to D2 and D3 receptors needs to be determined. Fifth, it has been shown that anesthesia can shift HA-state to LA-state and our preliminary anesthesia effects in vitro confirm this observation. However, it may not be an accurate representation of in vivo effects, since the concentrations used in vitro expose the brain slices to higher than the suggested minimum alveolar concentrations in vivo for

isoflurane. Additionally, anesthesia effects reported here have to be reconciled with reported in vivo results showing increased binding of agonists under anesthesia.

5 | SUMMARY

High-affinity state binding of the fluorine-18 labeled dopamine receptor agonists; ^{18}F-5-OH-FPPAT and ^{18}F-5-OH-FHXPAT have been demonstrated both in vitro and ex vivo. These findings thus suggest that in vivo PET measures of the agonists in brain regions at least in part reflects binding to the membrane-bound HA-state of the receptor. Because dopamine was able to displace the radiotracers to a greater degree compared with Gpp(NH)p, a process of receptor-radiotracer internalization may be occurring. This receptor-radiotracer complex is amenable to displacement by dopamine. Additionally, the Gpp(NH)p non-displaceable component may be D3 receptor bound. Our initial successful evaluation of ^{18}F-7-OH-FHXPAT will assist in the further evaluation of D3 receptor component.

Acknowledgments

This research study was supported by National Institute of Health grants NIH DA038886 (JM) and NIH EB006110 (JM). The authors like to thank Dr. Emiliana Borrelli for the D2R knock-out mice. Technical assistance of Drs. Baogang Xue, Sankha Chattopadhyay, Rama Pichika, and Reza Mirbolooki and Mai Tran, Sunny Shah, Kathy Kim, Arti Karmur, and Portia Trinidad is acknowledged.

Funding information

National Institute of Health grants NIH, Grant/Award Number: DA038886; NIH, Grant/Award Number: EB006110

References

Baik JH, Picetti R, Saiardi A, Thiriet G, Dierich A, Depaulis A, … Borrelli E. Parkinsonian-like locomotor impairment in mice lacking dopamine D2 receptors. Nature. 1995; 377:424–428. [PubMed: 7566118]

Constantinescu CC, Coleman RA, Pan ML, Mukherjee J. Striatal and extrastriatal microPET imaging of D2/D3 dopamine receptors in rat brain with *18*F-fallypride and *18*F-desmethoxyfallypride. Synapse. 2011; 65:778–787. [PubMed: 21218455]

Constantinescu CC, Mukherjee J. Performance evaluation of an Inveon PET preclinical scanner. Physics and Medicine and Biology. 2009; 54:2885–2899.

Finnema SJ, Halldin C, Bang-Andersen B, Gulyás B, Bundgaard C, Wikström HV, Farde L. Dopamine D(2/3) receptor occupancy of apomorphine in the nonhuman primate brain-a comparative PET study with [11C]raclopride and [11C]MNPA. Synapse. 2009; 63:378–389. [PubMed: 19173265]

Finnema SJ, Stepanov V, Nakao R, Sromek AW, Zhang T, Neumeyer JL, … Halldin C. 18F-MCL-524, an 18F-labeled dopamine D2 and D3 receptor agonist sensitive to dopamine: A preliminary study. Journal of Nuclear Medicine. 2014; 55:1164–1170. [PubMed: 24790219]

Garner SE, Kung MP, Foulon C, Chumpradit S, Kung HF. [125I](S)-trans-7-OH-PIPAT: a potential spect imaging agent for sigma binding sites. Life Sciences. 1994; 54:593–603. [PubMed: 8114613]

Gonzalez AM, Sibley DR. 3H-7-OH-DPAT is capable of labeling dopamine D2 as well as D3 receptors. European Journal of Pharmacology. 1995; 272:R1–R3. [PubMed: 7713138]

Grigoriadis D, Seeman P. Complete conversion of brain D-2 dopamine receptors from the high-to low-affinity state for dopamine agonists, using sodium ions and guanine nucleotide. Journal of Neurochemistry. 1985; 44:1925–1935. [PubMed: 3157782]

Hwang DR, Narendran R, Laruelle M. Positron-labeled dopamine agonists for probing the high affinity states of dopamine subtype 2 receptors. Bioconjugate Chemistry. 2005; 16:27–31. [PubMed: 15656572]

Joyce JN, Millan MJ. Dopamine D3 receptor antagonists as therapeutic agents. Drug Discovery Today. 2005; 10:917–925. [PubMed: 15993811]

Kung MP, Chumpradit S, Frederick D, Garner S, Burris KD, Molinoff PB, Kung HF. Characterization of binding sites for 125I-R-(+)trans-7-OH-PIPAT in rat brain. Naunyn-Schmiedeberg's Archives of Pharmacology. 1994; 350:611–617.

Le Foll B, Wilson AA, Graff A, Boileau I, Di Ciano P. Recent methods for measuring dopamine D3 receptor occupancy in vivo: Importance for drug development. Frontiers Pharmacology. 2014; 5:1–12.

Levesque D, Diaz J, Pilon C, Martres MP, Giros B, Souil E, … Sokoloff P. Identification, characterization, and localiztion of the dopamine D-3 receptor in rat brain using 7-[H-3]hydroxy-N °-di-n-propyl-2-aminotetralin. Proceedings of the National Academy of Sciences of the United States of America. 1992; 89:8155–8159. [PubMed: 1518841]

Ma Y, Smith D, Hof PR, Foerster B, Hamilton S, Blackband SJ, … Benveniste H. In vivo 3D digital atlas database of the adult C57BL/6J mouse brain by magnetic resonance microscopy. Frontiers in Neuroanatomy. 2008; 2:1. [PubMed: 18958199]

Mach RH, Tu Z, Xu J, Li S, Jones LA, Taylor M, … Mintun MA. Endogenous dopamine (DA) competes with the binding of a radiolabeled D3 receptor partial agonist in vivo: A positron emission tomopgraphy study. Synapse. 2011; 65:724–732. [PubMed: 21132811]

McCormick PN, Ginovart N, Wilson AA. Isoflurane anaesthesia differentially affects the amphetamine sensitivity of agonist and antagonist D2/D3 positron emission tomography radiotracers: Implications for in vivo imaging of dopamine release. Molecular Imaging and Biology. 2010; 13:737–746.

Mugnaimi M, Iavarone L, Cavallini P, Griffante C, Olisoi B, Savoia C. Occupancy of brain dopamine D3 receptor and drug craving: a translational approach. Neuropsychopharmacology. 2013; 38:302–312. [PubMed: 22968817]

Mukherjee J, Constantinescu CC, Hoang AT, Jerjian T, Majji D, Pan ML. Evaluation of ^{18}F-fallypride binding to dopamine D3 receptor subtype using in vitro and in vivo imaging in the rodent brain. Synapse. 2015; 69:577–591. [PubMed: 26422464]

Mukherjee J, Narayanan TK, Christian BT, Shi B, Dunigan K, Mantil J. In vitro and in vivo evaluation of the binding of the dopamine D-2 receptor agonist, 11C-(R°)–5-hydroxy-2-(di-n-propylamino) tetralin in rodents and non-human primate. Synapse. 2000; 37:64–70. [PubMed: 10842352]

Mukherjee J, Narayanan TK, Christian BT, Shi B, Yang ZY. Binding characteristics of high-affinity dopamine D2/D3 receptor agonists, ^{11}C-PPHT and ^{11}C-ZYY-339 in rodents and imaging in non-human primates by PET. Synapse. 2004; 54:83–89. [PubMed: 15352133]

Mukherjee J, Yang ZY, Lew R, Brown T, Kronmal S, Cooper M, Seiden LS. Evaluation of *d*-amphetamine effects on the binding of dopamine D-2 receptor radioligand, [F-18]fallypride in non-human primates using positron emission tomography. Synapse. 1997; 27:1–13. [PubMed: 9268060]

Munson PJ, Rodbard D. LIGAND: A versatile approach for the characterisation of ligand binding systems. Analytical Biochemistry. 1980; 107:220–239. [PubMed: 6254391]

Nobrega JN, Seeman P. Dopamine D-2 receptors mapped in rat brain with 3H(+)PHNO. Synapse. 1994; 17:167–172. [PubMed: 7974199]

Payer DE, Behzadi A, Kish SJ, Houle S, Wilson AA, Rusjan PM. Heightened D3 dopamine receptor levels in cocaine dependence and contributions to the addiction behavioral phenotype: A PET study with 11C-PHNO. Neuropsychopharmacology. 2014; 39:313–318.

Rabiner EA, Slifstein M, Nobrega J, Plisson C, Huiban M, Raymond R, … Laruelle MA. In vivo quantification of regional dopamine-D3 receptor binding potential of (+)-PHNO: Studies in non-human primates and transgenic mice. Synapse. 2009; 63:782–793. [PubMed: 19489048]

Seeman P. All roads to schizophrenia lead to dopamine super-sensitivity and elevated dopamine D2high receptors. CNS Neuroscience & Therapeutics. 2011; 17:118–132. [PubMed: 20560996]

Seeman P, Kapur S. Anesthetics inhibit high-affinity states of dopamine D2 and other G-linked receptors. Synapse. 2003; 50:35–60. [PubMed: 12872292]

Seeman P, Wilson A, Gmeiner P, Kapur S. Dopamine D2 and D3 receptors in human putamen, caudate nucleus, and globus pallidus. Synapse. 2006; 60:205–211. [PubMed: 16739118]

Shalgunov V, van Wieringen JP, Janssen HM, Fransen PM, Dierckx R, Michel MC, … Elsinga PH. Synthesis and evaluation in rats of homologous series of 18F-labeled dopamine D2/3 receptor agonists based on the 2-aminomethylchroman scaffold as potential PET tracers. EJNMMI Research. 2015a; 5:41.

Shalgunov V, van Wieringen JP, Janssen HM, Fransen PM, Dierckx R, Michel MC, … Elsinga PH. Synthesis and evaluation in rats of the dopamine D2/3 receptor agonist 18F-AMC20 as a potential radioligand for PET. Journal of Nuclear Medicine. 2015b; 56:133–139. [PubMed: 25476538]

Shi B, Narayanan TK, Christian BT, Chattopadhyay S, Mukherjee J. Synthesis and biological evaluation of the binding of dopamine D2/D3 receptor agonist, (R°)–5-hydroxy-2-(N-propyl-N-(5′-(18)F-fluoropentyl)aminotetralin ((18)F-5-OH-FPPAT) in rodents and nonhuman primates. Nuclear Medicine and Biology. 2004; 31:303–311. [PubMed: 15028242]

Shi B, Narayanan TK, Yang ZY, Christian BT, Mukherjee J. Radiosynthesis and in vitro evaluation of 2-(N-alkyl-N-1-11C-propyl)-aminotetralin analogs as high affinity dopamine D-2 receptor agonists for use as potential PET radiotracers. Nuclear Medicine and Biology. 1999; 26:725–735. [PubMed: 10628551]

Shotbolt P, Tziortzi AC, Searle GE, Colasanti A, van der Aart J, Abanades S, … Rabiner EA. Within subject comparison of 11C-(+)-PHNO and 11C-raclopride sensitivity to acute amphetamine challenge in healthy humans. Journal of Cerebral Blood Flow and Metabolism. 2012; 32:127–136. [PubMed: 21878947]

Skinbjerg M, Sibley DR, Javitch JA, Abi-Dargham A. Imaging the high-affinity state of the dopamine D2 receptor in vivo: Fact or fiction. Biochemical Pharmacology. 2012; 83:193–198. [PubMed: 21945484]

Sromek AW, Zhang S, Akurathi V, Packard AB, Li W, Alagille D, … Neumeyer JL. Convenient synthesis of 18F-radiolabeled R-(−)-N-n-propyl-2-(3-fluoropropanoxy-11-hydroxynorapomorphine. Journal of Labelled Compounds and Radiopharmaceuticals. 2014; 57:725–729. [PubMed: 25400260]

Tziortzi AC, Searle GE, Tzimopoulou S, Salinas C, Beaver JD, Jenkinson M, … Gunn RN. Imaging dopamine receptors in humans with [11C]-(+)-PHNO: Dissection of D3 signal and anatomy. Neuroimage. 2011; 54:264–277. [PubMed: 20600980]

Van Vliet LA, Tepper PG, Dijkstra D, Damsma G, Wikstrom H, Pugsley TA, … Wise LD. Affinity for dopamine D2, D3, and D4 receptors of 2-aminotetralins. Relevance of D2 agonist binding for determination of receptor subtype selectivity. Journal of Medicinal Chemistry. 1996; 39:4233–4237. [PubMed: 8863800]

Vanhauwe JF, Josson K, Luyten WH, Driessen AJ, Leysen JE. G-protein sensitivity of ligand binding to human dopamine D2 and D3 receptors expressed in Escherichia coli: Clues for a constrained D3 receptor structure. Journal of Pharmacology and Experimental Therapeutics. 2000; 295:274–283. [PubMed: 10991990]

Vuckovic MG, Li Q, Fisher B, Nacca A, Leahy RM, Walsh JP, … Petzinger GM. High intensity treadmill exercise upregulates striatal dopamine D2 receptor in 1-methyl-4-phenyl-1,2,3,6-tetrahydropyridine-lesioned mice: in vivo PET-imaging with ^{18}F-fallypride. Movement Disorders. 2010; 25:2777–2784. [PubMed: 20960487]

Willeit M, Ginovart N, Kapur S, Houle S, Hussey D, Seeman P, Wilson AA. High affinity states of human brain dopamine D2/3 receptors imaged by the agonist 11C-(+)PHNO. Biol Psychiatry. 2006; 59:389–394. [PubMed: 16373068]

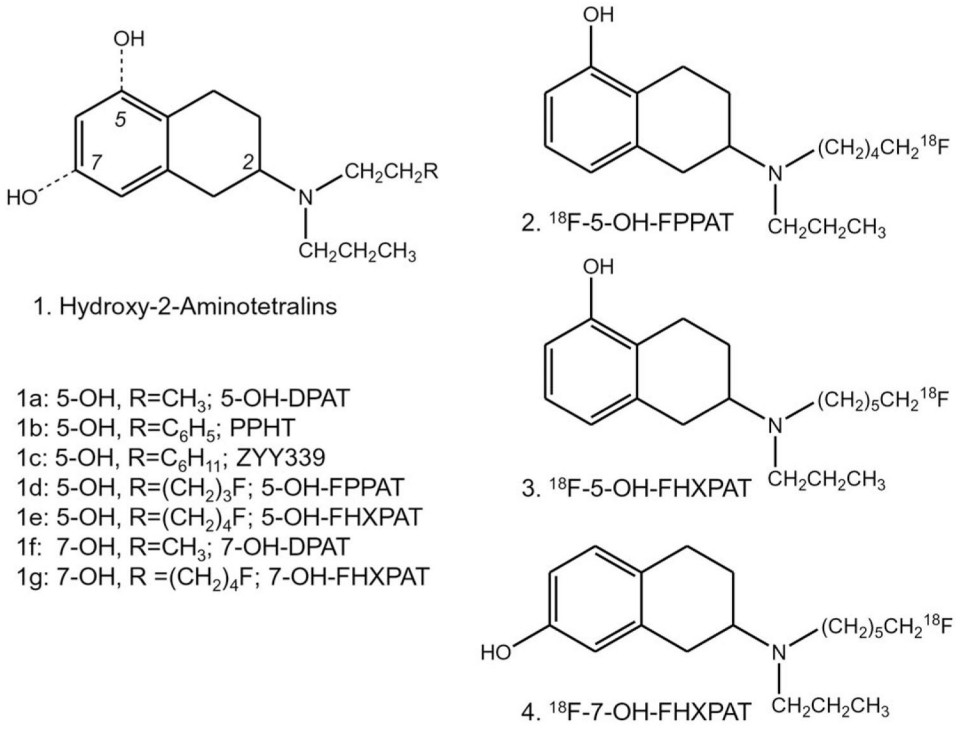

FIGURE 1.

Successful Dopamine D2 and D3 Receptor 2-Aminotetralin Agonists. Chemical structures of hydroxy-2-aminoteralin derivatives pursued as ^{11}C- and ^{18}F-labeled imaging agents (**a**–**g**). Fluorine-18 labeled agonists include: 5-hydroxy-2-(*N*-propyl-*N*-(5-^{18}F-fluoropentyl) aminotetralin (^{18}F-5-OH-FPPAT, **2**), 5-hydroxy-2-(*N*-propyl-*N*-(5′-^{18}F-fluorohexyl)aminotetralin (^{18}F-5-OH-FHXPAT, **3**), and 7-hydroxy-2- (*N*-propyl-*N*-(5′-^{18}F-fluorohexyl)aminotetralin (^{18}F-7-OH-FHXPAT, **4**)

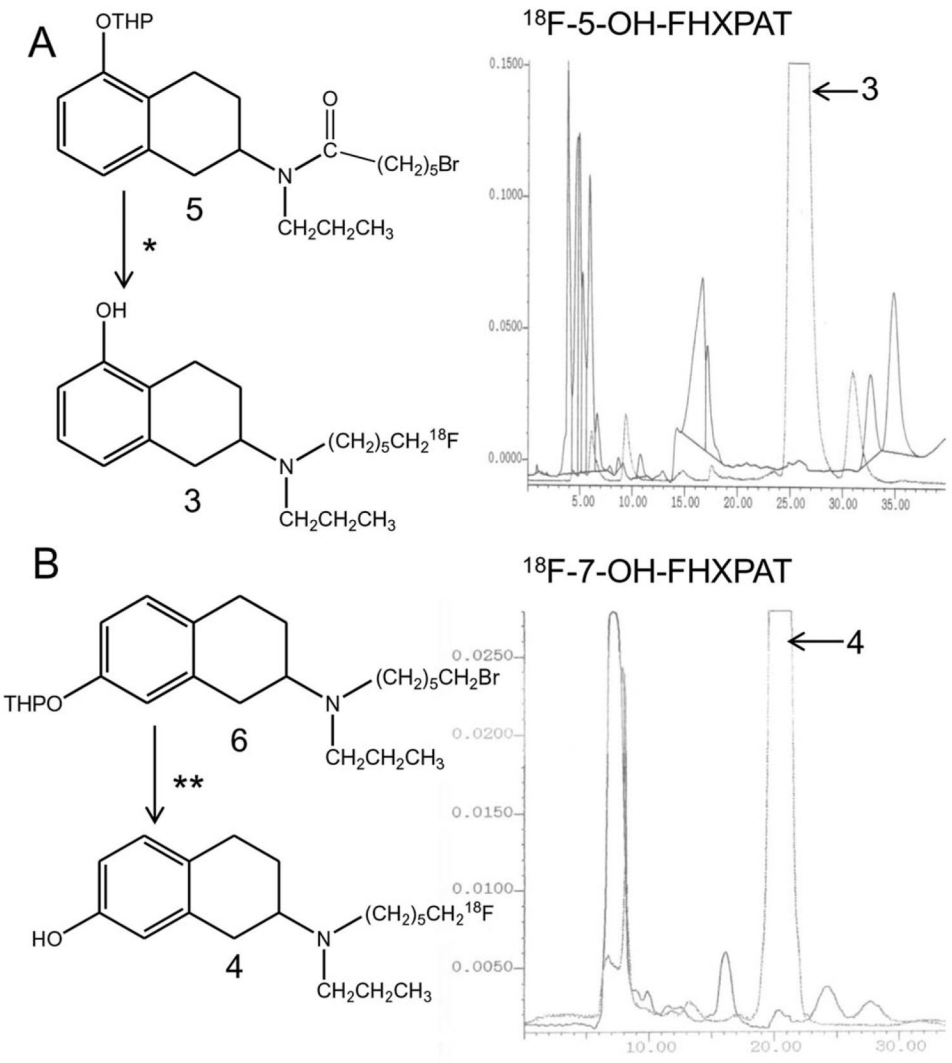

FIGURE 2.

Radiosynthesis of ^{18}F-5-OH-FHXPAT and ^{18}F-7-OH-FHXPAT. (**a)** Radiosynthesis scheme for ^{18}F-5-OH-FHXPAT and C18 reverse phase HPLC chromatogram showing separation profile of ^{18}F-5-OH-FHXPAT. Reagents *: Brominated precursor **5** was reacted with 1. ^{18}F-fluoride, Kryptofix, potassium carbonate in acetonitrile; 2. Lithium aluminum hydride in tetrahydrofuran; 3. Aqueous HCl in methanol. The predominant radioactive peak at 25–27 min is ^{18}F-5-OH-FHXPAT. (**b)** Radiosynthesis scheme for ^{18}F-7-OH-FHXPAT and C18 reverse phase HPLC chromatogram showing separation profile of ^{18}F-7-OH-FHXPAT. Reagents **: Brominated precursor **6** was reacted with 1. ^{18}F-fluoride, Kryptofix, potassium carbonate in acetonitrile; 2. Aqueous HCl in methanol. The predominant radioactive peak at 20–22 min is ^{18}F-7-OH-FHXPAT

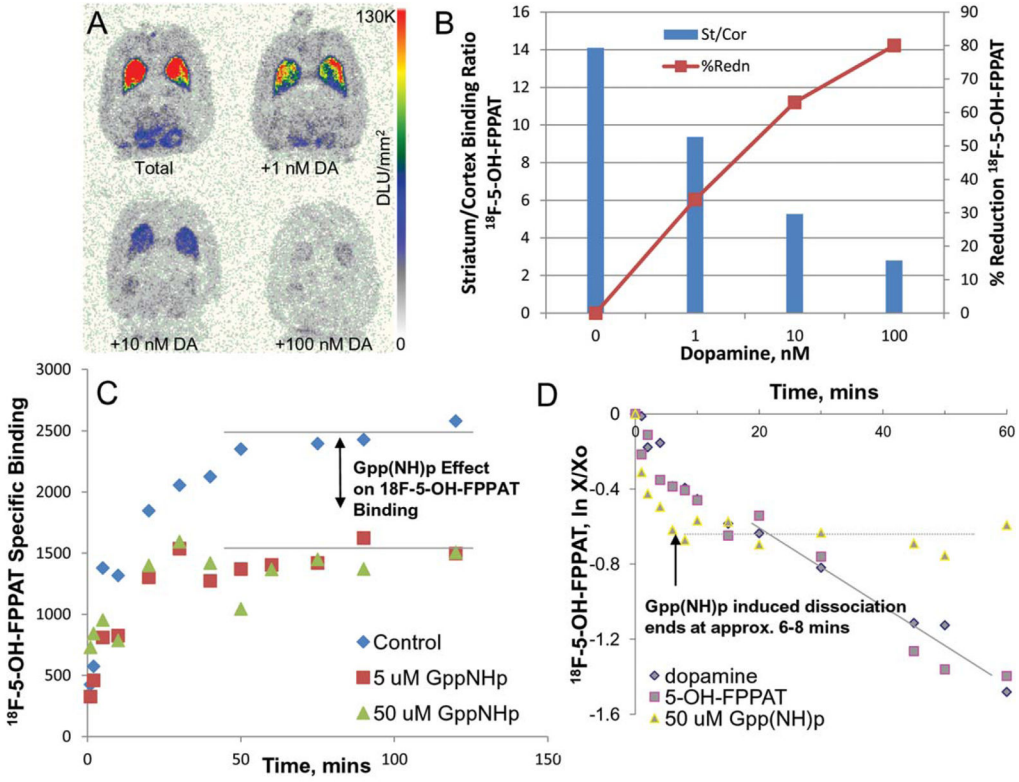

FIGURE 3.

In Vitro ^{18}F-5-OH-FPPAT Studies: (**a)** Dopamine competition with ^{18}F-5-OH-FPPAT in rat brain horizontal sections. (**b)** Plot showing >50% reduction of ^{18}F-5-OH-FPPAT in striata with 10 nM dopamine. (**c)** Association of ^{18}F-5-OH-FPPAT in rat striatal tissue homogenate incubated for up to 120 min at 25°C in the absence or presence of GppNHp (5 and 50 μM). Residual binding of up to 50–60% remained in the presence of Gpp(NH)p. (**d)** Dissociation of ^{18}F-5-OH-FPPAT in rat striatal tissue homogenate incubated with ^{18}F-5-OH-FPPAT for 60 min at 25°C. Dissociation initiated by DA (100 μM), FPPAT (10 μM) or GppNHp (50 μM) at different times found rates of dissociation to be 0.02 min^{-1} (80% displaced), 0.02 min^{-1} (80% displaced), and 0.05 min^{-1} (45% displaced), respectively

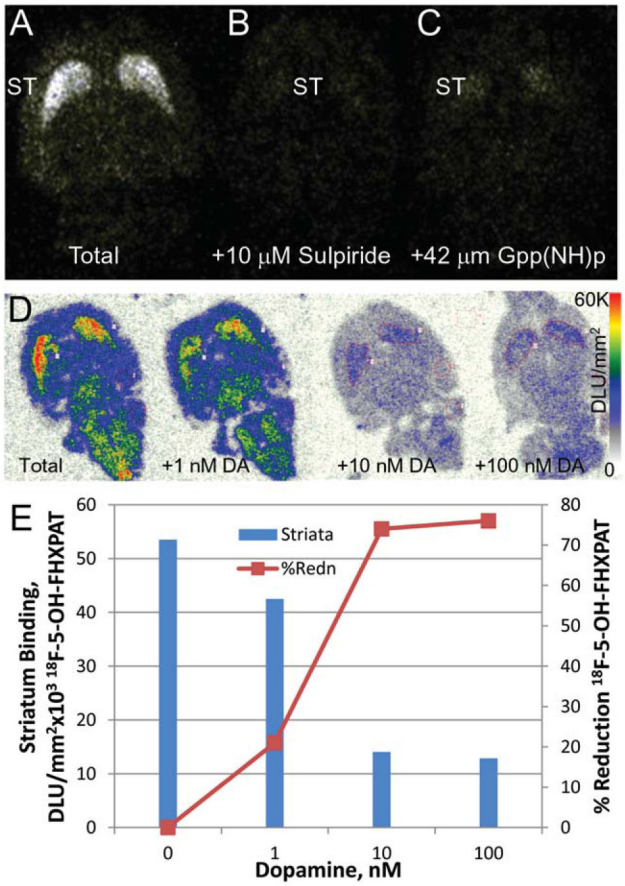

FIGURE 4.

In Vitro ^{18}F-5-OH-FHXPAT Studies: (**a)** Total binding of ^{18}F-5-OH-FHXPAT to rat brain slice (10 μm thick) showing predominant binding in the striatum (ST). (**b)** Nonspecific binding in the presence of D2/D3 antagonist, 10 μM sulpiride. (**c)** Decrease of ^{18}F-5-OH-FHXPAT binding in the presence of 42 μM Gpp(NH)p. (**d)** Dopamine competition with ^{18}F-5-OH-FPPAT in rat brain horizontal sections. (**e)** Plot showing >50% reduction of ^{18}F-5-OH-FPPAT in striata with 10 nM dopamine

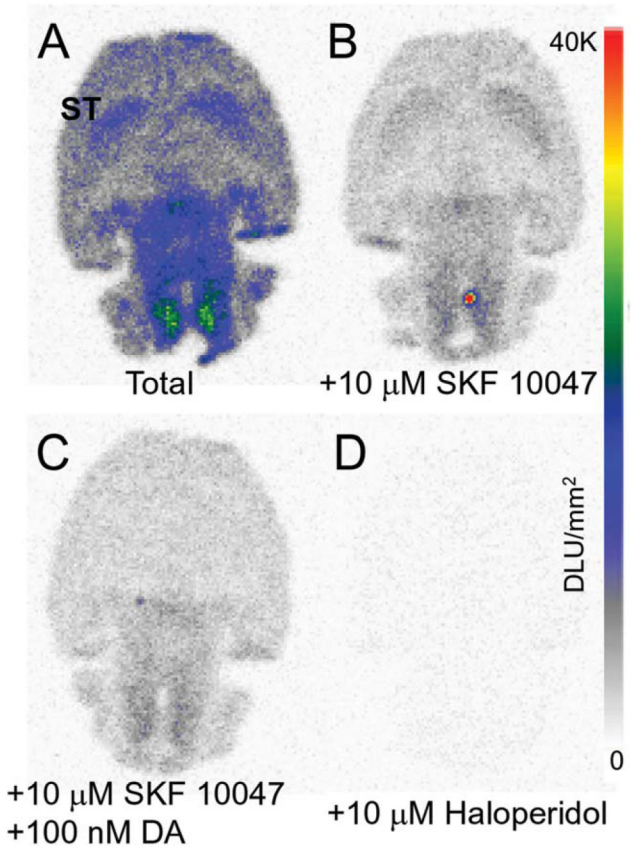

FIGURE 5.

In Vitro ^{18}F-7-OH-FHXPAT Studies. In vitro autoradiographs of rat brain horizontal slices (10 μm thick) incubated with 111 kBq/cc at 37°C, showing (**a**). Total binding of ^{18}F-7-OH-FHXPAT. (**b**). Binding of ^{18}F-7-OH-FHXPAT in the presence of 10 μM SKF10047 (55% binding was reduced over the various brain regions). (**c**). Binding of ^{18}F-7-OH-FHXPAT in the presence of SKF10047 and dopamine (56% of the striatal binding was reduced) and (**d**). Nonspecific binding of ^{18}F-7-OH-FHXPAT in the presence of 10 μM haloperidol (>95% binding of ^{18}F-7-OH-FHXPAT was displaced)

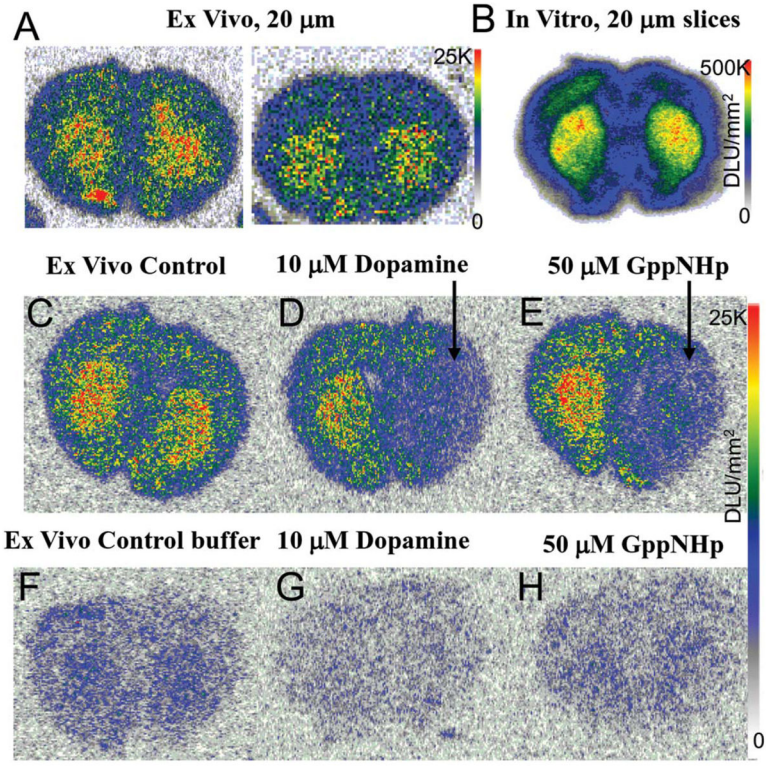

FIGURE 6.

Ex Vivo ^{18}F-5-OH-FHXPAT Studies: (**a)** Rats injected with ~7 MBq of ^{18}F-5-OH-FHXPAT and killed at 25 min postinjection. Coronal brain slices (20 µm) were obtained showing greater binding in striatum (ST), with striata to cortex ratio of 1.5–1.6. (**b)** In vitro binding observed in rat brain coronal sections incubated with ^{18}F-5-OH-FHXPAT at 37°C for 30 min. (**c–e)** Ex vivo coronal sections showing total binding at 25 min post injection (**c**), 10 µM dopamine applied for 5 min to the right half displacing ^{18}F-5-OH-FHXPAT from the striata (**d**) and 50 µM Gpp(NH)p applied for 5 min to the right half displacing ^{18}F-5-OH-FHXPAT from the striata (**e**). (**f–h)** Ex vivo coronal sections obtained 25 min postinjection showing 12 min buffer-treated total binding (**f**), buffer containing 10 µM dopamine treatment reduced binding by >80% (**g**) and buffer containing 50 µM Gpp(NH)p treatment, which reduced binding by >45% (**h**)

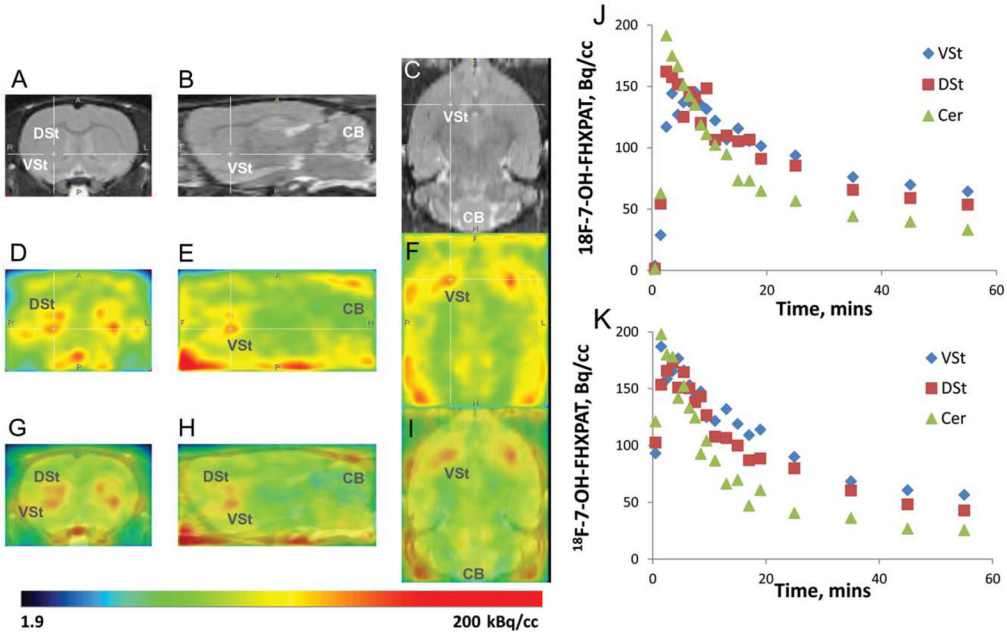

FIGURE 7.

In Vivo Rat PET with ^{18}F-7-OH-FHXPAT. Normal male Sprague-Dawley rats injected intravenously with 7 MBq of ^{18}F-7-OH-FHXPAT. Summed PET images were coregistered with rat MRI template. (**a–c**) MR sections, coronal (**a**), saggital (**b**), and horizontal (**c**) showing DStr, VSt (cross hairs), and cerebellum (CB). (**d–f**) PET image slices corresponding to MR slices; coronal (**d**), sagittal (**e**), and horizontal (**f**) showing binding of ^{18}F-7-OH-FHXPAT in DSt and VSt. (**g–i**) Corresponding coregistered PET-MR images showing binding of ^{18}F-7-OH-FHXPAT in DSt and VSt and little in CB

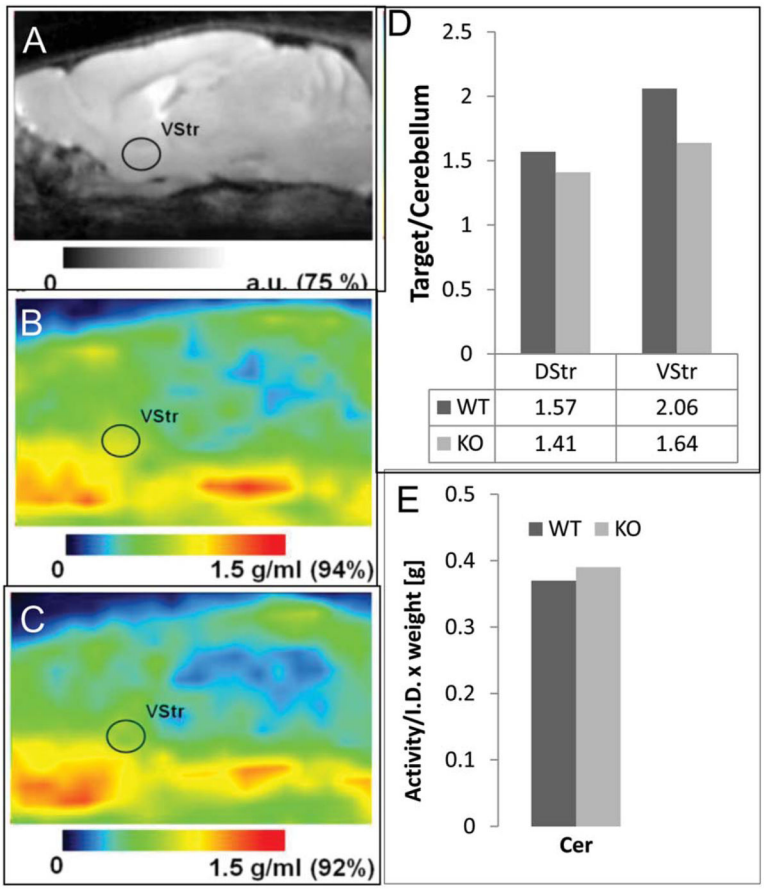

FIGURE 8.

In Vivo Mice PET with ^{18}F-7-OH-FHXPAT. (**a**) Sagital sections of the MR mouse brain template. (**b**) ^{18}F-7-OH-FHXPAT images of the WT mouse. (**c**). D2 knock out (KO) mouse. Right VStr is indicated on all three images. Color bars show the scale of the images presented in arbitrary units (a.u., MR) and standard uptake value units (g/mL, PET). Mice were injected with 2.0 MBq of ^{18}F-7-OH-FHXPAT and scanned for 30 min starting at 30 min post tracer injection. Anesthesia was maintained with 2.5% isoflurane. (**d**) Target to cerebellum ratios of ^{18}F-7-OH-FHXPAT for DStr, VStr in both WT (n=2), and KO (n=2) mouse. (**e**). Cerebellum activity normalized to injected activity and animal weight (in grams) in both WT and KO mice

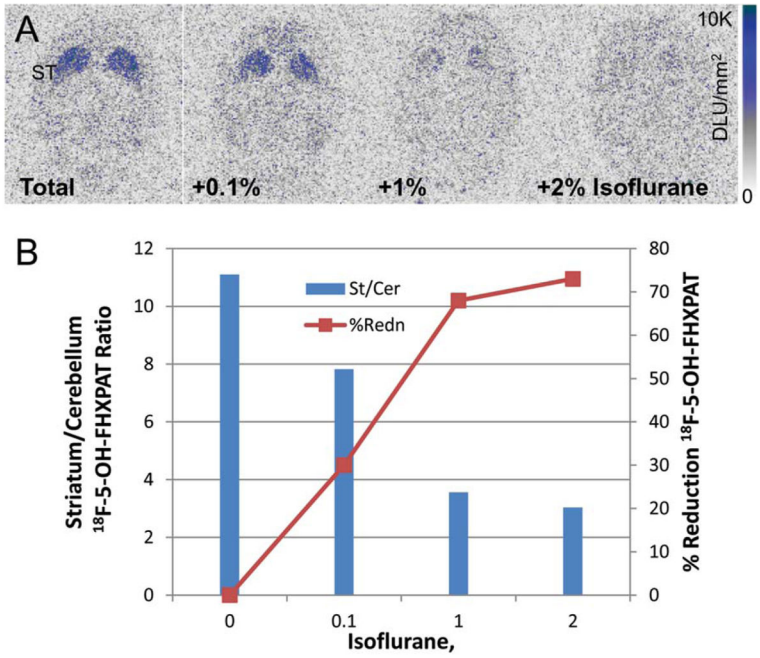

FIGURE 9.

In Vitro ^{18}F-5-OH-FHXPAT Isoflurane Effects: (**a**) Sprague-Dawley brain slices (20 μm) were preincubated with either buffer or buffer containing 0.1, 1, and 2% isoflurane for 15 min. Slices were then incubated in the above buffers in presence of 15 kBq/cc ^{18}F-5-OH-FHXPAT at 37°C for 1 hr. (**b**) Plot showing a reduction in ^{18}F-5-OH-FHXPAT binding of 30 at 0.1% and >65% at 1% isoflurane

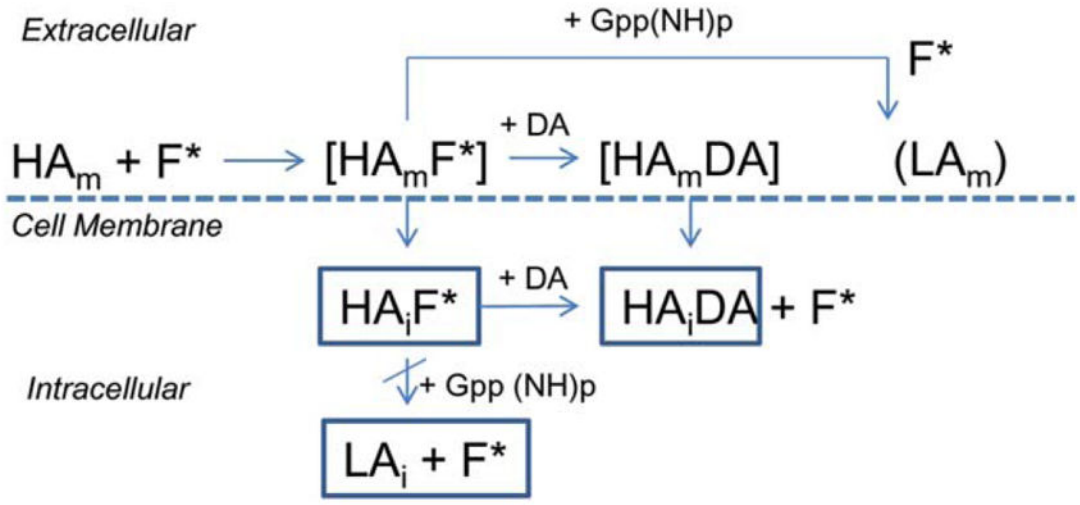

FIGURE 10.

Schematic showing plausible internalization of ^{18}F-fluoroaminotetralins: High-affinity state membrane bound D2 and D3 dopamine receptor (HA_m) binds ^{18}F-fluorinated Aminotetralins (F*) observed in our in vitro and ex vivo studies (HA_mF^*). Dopamine (DA) displaces F* to form (HA_mDA), but 5′-Guanylyl imidodiphosphate (Gpp(NH)p) displaces F* partially by converting HA_m to LA state membrane bound dopamine receptor (LA_m). Partial conversion may be due to internalized high-affinity state dopamine receptor (HA_i) with bound F* (HA_iF^*), where DA is able to displace F* to form HA_iDA, while Gpp(NH)p has little effect on the internalized HA_iF^*